JOURNAL OF MATERIALS SCIENCE 16 (1981) 237–250

The effect of minor additions of titanium on the fracture toughness of Fe-12 at % Ni alloys at -196° C

H. CONRAD, C. YIN, G. A. SARGENT
Metallurgical Engineering and Materials Science Department, University of Kentucky, Lexington, KY 40506, USA

The reasons for the improvement in the fracture toughness of an Fe–12 at % Ni base alloy at – 196° C by the addition of small amounts of Ti were investigated employing transmission electron microscopy (TEM), scanning electron microscopy (SEM) and Auger electron spectroscopy. Ti additions ranging from 0.18 to 0.99 at % and heat treatments of 2 h at 550, 685 and 820° C respectively followed by a water quench were considered, since previous work by Witzke and Stephens had shown that maximum K_{IC} occurred for an Fe–12 at % Ni–0.18 at % Ti alloy heat treated at 685° C. It was found here that K_{IC} at – 196° C for all the alloys and heat treatments correlated with the fraction of ductile fracture compared to intergranular and cleavage fracture, the latter modes being predominant in the Fe–12 at % Ni base alloy without Ti additions. Cubic and rectangular shaped inclusions were noted in the SEM fractographs of the alloys with the Ti additions. A fine precipitate was observed by TEM for the Fe–12 at % Ni–0.18 at % Ti alloy heat treated at 550° C; this precipitate was not observed for the 685 and 820° C heat treatments of the same alloy. Auger mappings of the fracture surfaces indicated a weak to moderate association of the interstitials C, N and O with Ti, the degree of which depended on the particular interstitial and the heat treatment temperature. It was concluded that the increase in K_{IC} due to the initial 0.18 at % addition of Ti was due to a scavenging of interstitials which normally segregate at the grain boundaries and to the refinement of the microstructure. The subsequent decrease in K_{IC} with further Ti additions was attributed to the increase in flow stress and slight lowering of the fracture stress resulting from these additions. It was further inferred that the Ti additions and heat treatment on the flow and fracture stresses may be due in a large part to their influence on the amount, size and distribution of the precipitate which was observed.

1. Introduction

One of the factors to be considered in the development of iron base alloys for cryogenic applications is the detrimental effect on toughness of impurity elements such as oxygen, nitrogen and sulfur [1–4]. This problem is generally controlled by adding reactive metals to the melt which combine with these impuirities and thereby reduce or eliminate their detrimental effect. Recognizing this, Witzke and Stephens [5] investigated the effects of minor additions (up to 4 at %) of eleven reactive metals on the tensile properties and fracture toughness of a binary Fe–12 at % Ni base alloy. This base alloy was chosen because prior work by Jin *et al.* [6] indicated that an Fe–12 at % Ni alloy with titanium additions was ductile at 78 K. In their study Witzke and Stephens [5] found that Al, Ti, V, Nb and Ta improved the fracture toughness of the Fe–12 at % Ni alloy at – 196° C; Zr, Hf, Ce, La and Y were less effective and Si had no effect. Further, they found that the toughness was dependent on the concentration of the reactive metal (peaking sharply at a relatively small concentration for most additions) and the heat treatment employed (in the range of 550 to 820° C followed by a water quench). Concurrent optical and transmission

0022–2461/81/010237–14$03.40/0

electron microscopy (TEM) studies by them indicate that: (a) substructure plays a minor role in fracture toughness and (b) precipitate particles were not generally observed except in those alloys containing strong carbide-forming additions such as Hf and Ta. Scanning electron microscopy (SEM) examination of the fracture surfaces of the broken fracture toughness specimens revealed that ductile fracture (dimpled rupture) occurred in varying degrees, being most evident in the toughest materials.

The work of Witzke and Stephens [5] thus clearly established that significant improvements can be obtained in the fracture toughness of the Fe–12 at % Ni alloy by the minor additions of certain reactive metals, especially Al, Ti and Nb. However, the nature of the gettering which leads to the improved fracture toughness was not clearly ascertained, nor was the reason for the strong influence of the heat treatment. The present investigation was therefore undertaken to provide additional information regarding these two unresolved questions. A better understanding of these aspects of the subject is important in optimizing the beneficial effects of the reactive metal additions and in providing guidelines for the development of improved alloys.

The approach taken in this investigation was to characterize in more detail the microstructure (using TEM), solute distribution (using Auger electron spectroscopy) and fracture surface morphology (using SEM) of the tensile and slow bend fracture toughness specimens which had been previously tested by Witzke and Stephens [5] and which were made available to the present authors. The initial studies focused on the Fe–12 at % Ni–x at % Ti alloys because: (a) a large increase in the fracture toughness of the Fe–12 at % Ni base alloy had been obtained by the addition of titanium, (b) a significant effect of heat treatment on the fracture toughness had occurred and (c) preliminary SEM examination of the fracture surface of broken fracture toughness specimens by the present authors revealed a number of inclusions within the dimples of the ductile fracture regions.

The titanium additions considered in this study ranged from 0 to 1.0 at % and the heat treatments consisted of 2 h at 550, 685 and 820° C respectively, followed by a water quench. Within this range of composition and heat treatments, Witzke and Stephens [5] found that maximum fracture toughness occurred for the addition of 0.15 wt % (0.18 at %) Ti combined with the 685° C heat treatment.

2. Experimental procedure

2.1. Materials

The Fe–12 at % Ni and Fe–12 at % Ni–x at % Ti alloy tensile and notch bend fracture toughness specimens considered here (chemical compositions of which are given in Table I) were provided by Witzke and Stephens; the preparation, heat treatment and testing procedure of the specimens have been presented by nonconsumable arc melting in an argon atmosphere from high purity Fe, Ni and Ti. To adequately homogenize the ingots, each alloy was given a minimum of four melts. The ingots were hot rolled at 1100° C to the desired thickness (7 mm for the notch bend specimens and 1 mm for the tensile test specimens) and air cooled to room temperature. Tensile and notch bend specimens cut from the rolled sheet were then heat treated for 2 h at 550, 685 and 820° C respectively, followed by a water quench. According to the Fe–Ni phase transformation diagram for continuous heating or cooling shown in Fig. 1, the temperatures of the heat treatments are in the α, $\alpha + \gamma$ and γ phase fields respectively. Differential thermal analysis [7–9] indicates that the Ti additions of 0.18 and 0.99 at % considered here are not expected to appreciably alter the phase transformation diagram.

TABLE I Chemical composition of the materials

Specimen number	Metal content						Interstitial content		
	Fe		Ni		Ti		O	N	C
	wt %	at %	wt %	at %	wt %	at %	ppm (wt)		
C–974–T	87.60	88.10	12.40	11.90	0	0	160	41	26
D–367–T	87.15	87.67	12.70	12.15	0.15	0.18	61	12	18
D–27–T	86.65	87.33	12.75	12.20	0.40	0.47	68	13	25
D141–T	86.40	86.81	12.76	12.20	0.84	0.99	63	28	36

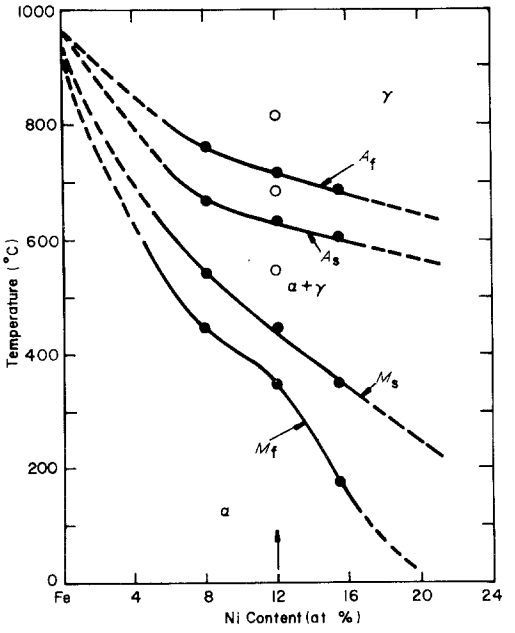

Figure 1 Phase transformation diagram for heating and cooling of Fe–Ni alloys [8].

2.2. Transmission electron microscopy

Transverse sections with a thickness of 0.38 mm were cut from the broken notch bend specimens and mounted on the flat surface of a ceramic circular disk with double stick Scotch tape. The specimens were then polished on both sides using silicon carbide papers going from 240 to 600 grit, under flowing water, to a thickness of about ~ 0.15 mm, following which they were chemically polished in a solution of 5 vol% hydrofluoric acid in 95 vol% H_2O_2 to a thickness of ~ 0.10 mm. Thin foil samples suitable for TEM examination were then prepared from these specimens by the Fischione twin-jet polisher using an electrolyte of 250 ml methanol, 150 ml butyl alcohol and 20 ml perchloric acid.

2.3. Scanning electron microscopy

One of the broken halves of the notch bend fracture toughness specimens was mounted on the standard specimen holder of a Phillips Stereoscon-Mark 2A SEM, using a silver paste as the mounting glue to avoid build-up of a surface charge. The fracture surface of the specimen was then examined with the emissive mode operated at 25 kV and with the primary beam normal to the surface. The percentage of ductile fracture (compared to intergranular and cleavage) and the dimple size of the ductile fracture regions were determined from SEM photomicrographs. The dimple size was measured by the linear intercept method on those micrographs which were considered to be most representative of the morphology of the fracture surface. The percentage of ductile fracture (characterized by the occurrence of dimples) was obtained by scanning the entire fracture surface of a specimen at a constant magnification and then averaging the percentage of ductile fracture estimated for each scan area.

2.4. Auger electron spectroscopy (AES)

A Varian Auger Electron spectrometer system was used to examine the fracture surfaces of the notch bend specimens. Since a suitable electron image of the fracture surface could not be obtained with the scanning sample positioner and TV monitor, a random area of the fracture surface was chosen for Auger spectrum analysis and Auger elemental image mapping. Further, since the fracture surfaces had been exposed to the atmosphere for some time prior to the Auger analysis, a technique developed by Palmberg [10], which consists of simultaneous ion bombardment and AES analysis, was employed to remove the influence of any contamination which may have occurred. The basic procedures used here to obtain the final Auger image mapping for the elements C, N, O, Ti, Ni and Fe on a particular selected area of fracture surface were then in general as follows:

(a) The fracture surface of a notch bend specimen was mounted on the carrousel sample holder located in the centre of a bell-jar. The bell-jar system was then evacuated to a pressure of 3×10^{-8} torr or better.

(b) The fracture surface normal was aligned parallel to the primary beam, which was generated by the 10 keV integral electron gun. Therefore, the angle between the fracture surface normal and the axis of ion bombardment gun was about 60°.

(c) The axial position of the sample was adjusted with respect to the Cylindrical Mirror Analyser (MA) to obtain a maximum, properly shaped, elastic peak and a measure of the instrumental line width (ILW).

(d) After the ILW was defined on a selected surface area, a complete scan of the Auger spectra for specific elements was performed with a primary beam energy of 6.5 keV, filament current of 2.90 A and high voltage output of 1200 V. A typical scan is shown in Fig. 2, which gives a plot of the Auger spectra for C and O at a particular

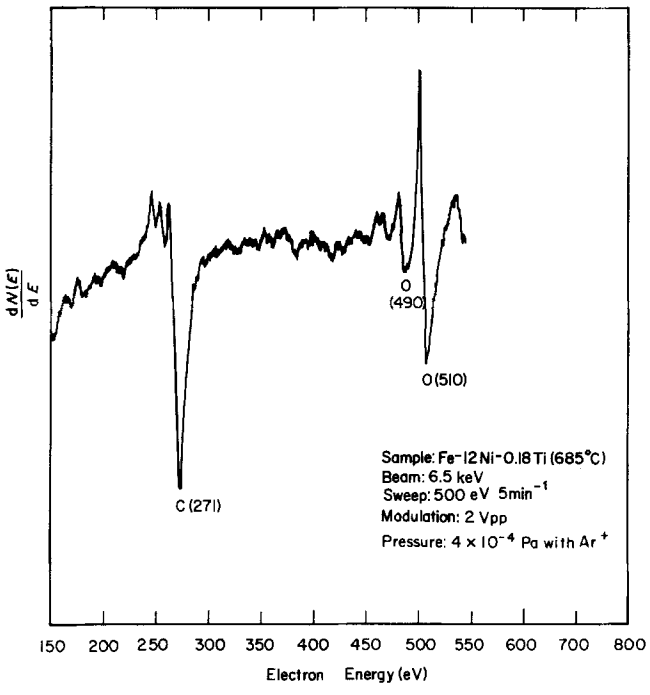

Figure 2 Auger spectra for C and O from fracture surface of Fe–12 at% Ni–0.81 at% Ti alloys heat treated at 685° C and tested at −196° C.

area on the fracture surface of the Fe–12 at% Ni–0.18 at% Ti alloy heat-treated at 685° C.

(e) Finally, the Auger elemental image mapping for a fixed Auger electron energy associated with a particular element (for example, O at E = 510 eV or 490 eV) was obtained by switching the CMA unit to the Auger mapping controlled unit, thereby yielding a map of the distribution of that element on the fracture surface. The mappings were photographed (representing a magnification of x 175) only after about 1 h of ion bombardment.

3. Results

3.1. Mechanical properties

The true stress–true strain curves (derived from data provided by Witzke and Stephens) for the tensile tests at 77 K on the Fe–12 at% Ni–x at% Ti alloys are presented in Fig. 3. Tensile properties extracted from these curves are plotted as a function of Ti content in Fig. 4. It should be noted that the yield stress, σ_{YS} increases significantly with Ti content for the 500° C heat treatment, but does not change appreciably for the 685 and 820° C treatments. On the other hand the ultimate tensile strength, σ_{UTS} increases with Ti content for all three heat treatments, the effect being however somewhat larger for the 550° C treatment than for the other two. The true fracture stress, σ_F increases appreciably with the addition of 0.15 wt% (0.18 at%) Ti for all three heat treatment temperatures; further increase in Ti content generally leads to a slight decrease in σ_F. In general, σ_F tends to increase slightly with increase in heat treatment temperature for all alloy compositions.

It should also be noted in Fig. 4 that ductility indicators such as the uniform elongation ϵ_u, the true fracture strain ϵ_F and the strain hardening exponent $n = d \ln \sigma / d \ln \epsilon$ all go through a maximum at 0.15 wt% (0.18 at%) Ti. Considering the effect of heat treatment, the 550° C treatment yields higher values of ϵ_u and n than does the 685 or 820° C treatment, whereas the reverse is true for ϵ_F.

The fracture toughness values obtained by Witzke and Stephens [5] are presented as a function of Ti content and heat treatment in Fig. 5. Similar to the ductility indicators, a maximum in K_{IC} occurs for the addition of 0.15 wt% (0.18 at%) Ti. Of the three heat treatments, the 685° C treatment yields the largest value of K_{IC} and the 550° C treatment the lowest. Thus, of the three tensile test ductility indicators, the true strain at fracture ϵ_F correlates best with fracture toughness.

Also included in Fig. 5 is the work to fracture, W_F given by the area under the true stress–true strain curves of Fig. 3. It should be noted that the effects of Ti and heat treatment on W_F are similar

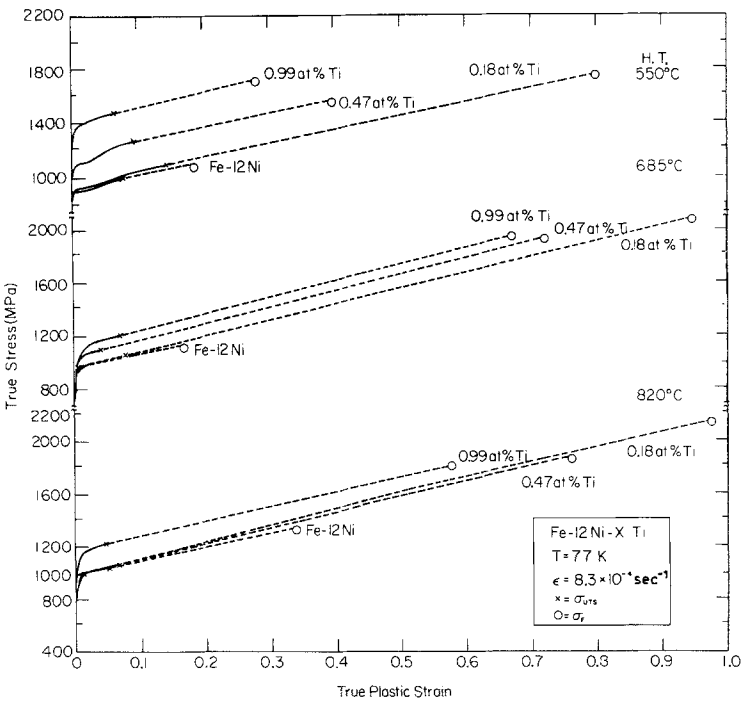

Figure 3 True stress–true strain curves of Fe–12 at % Ni–x at % Ti alloys heat treated at 550, 685 and 820° C.

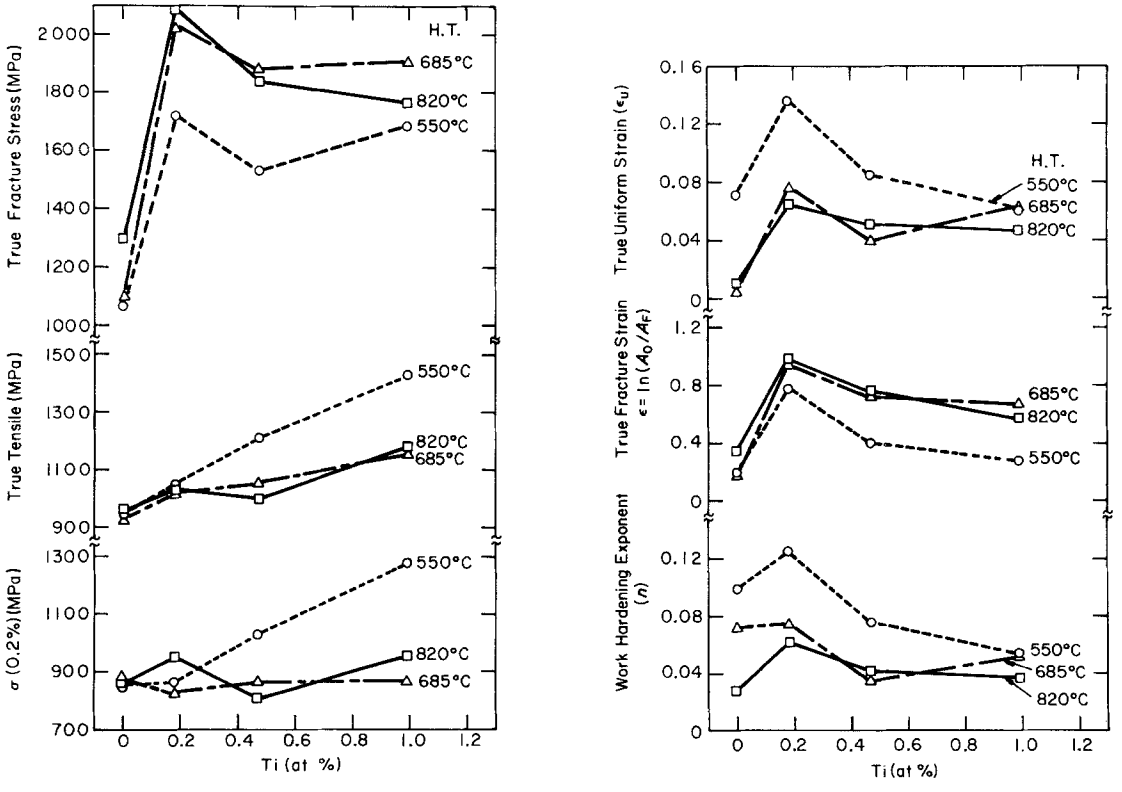

Figure 4 Tensile properties at −196° C of Fe–12 at % Ni–x at % Ti alloys against Ti content as a function of heat treatment temperature.

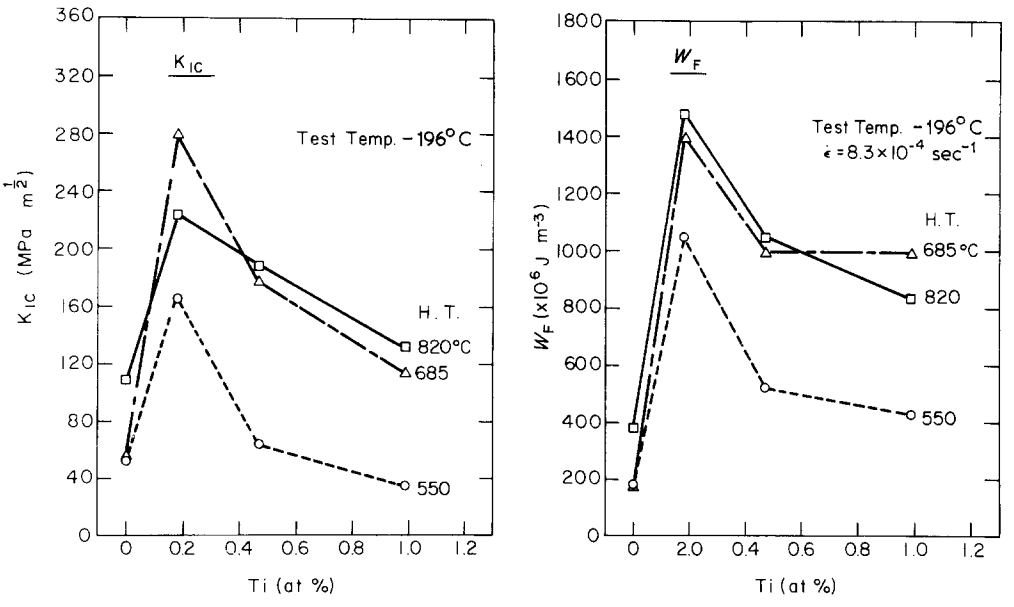

Figure 5 (a) K_{IC} and (b) work to fracture in tension W_F at − 196° C against Ti content as a function of heat treatment temperature.

to those on K_{IC}. This correlation is further evident in Fig. 6 where K_{IC} is plotted against W_F for the various Ti additions and heat treatments.

3.2. Scanning electron microscopy (SEM)

SEM fractographs of the fracture surfaces of the tensile and fracture toughness specimens tested at 77 K are presented in Figs 7 to 9. Pertinent features of the structures are summarized in Tables II and III. A good fraction of the fracture surface area of the fracture toughness specimens consists of intergranular and/or cleavage fracture. These brittle fracture modes also occurred in most of the tensile specimens, exceptions being the Fe–12 at % Ni–0.18 at % Ti alloy heat treated at all three temperatures and Fe–12 at % Ni–0.47 at % Ti

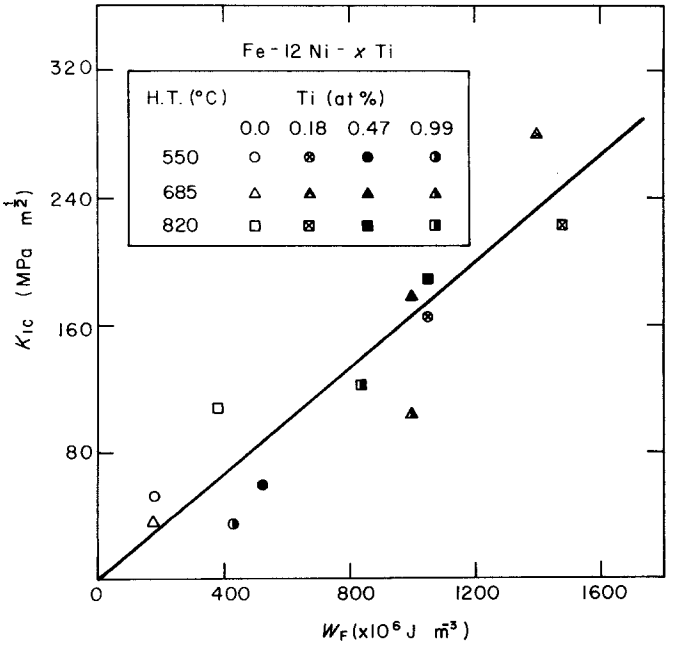

Figure 6 K_{IC} against W_F at − 196° C for Fe–12 at % Ni–x at % Ti alloys heat treated at 550, 685 and 820° C.

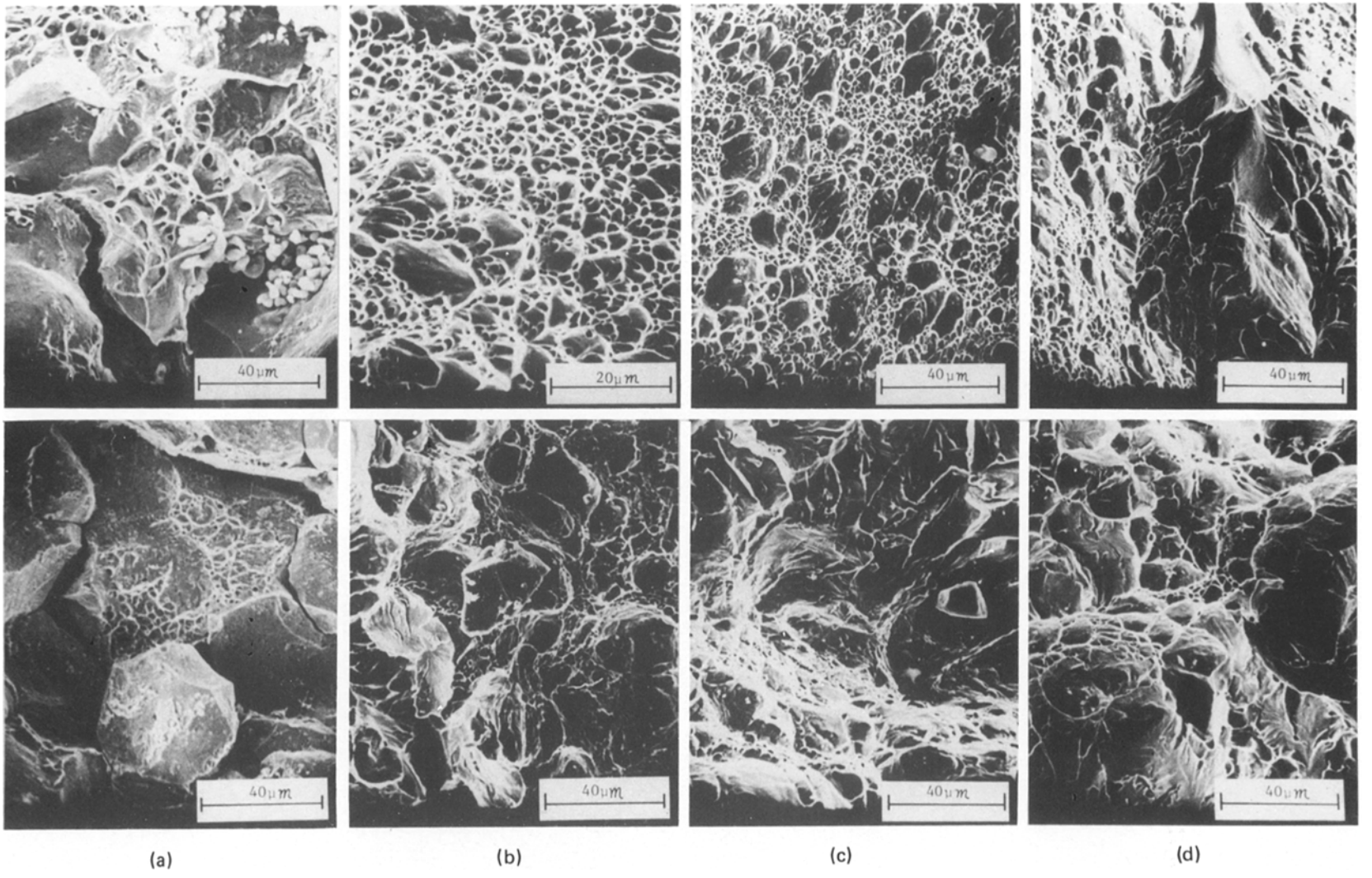

Figure 7 SEM fractographs from tensile specimens (upper) and notch bend specimens (lower) of (a) Fe–12 at % Ni, (b) Fe–12 at % Ni–0.18 at % Ti, (c) Fe–12 at % Ni–0.47 at % Ti, and (d) Fe–12 at % Ni–0.99 at % Ti alloys heat treated at 820° C and tested at – 196° C.

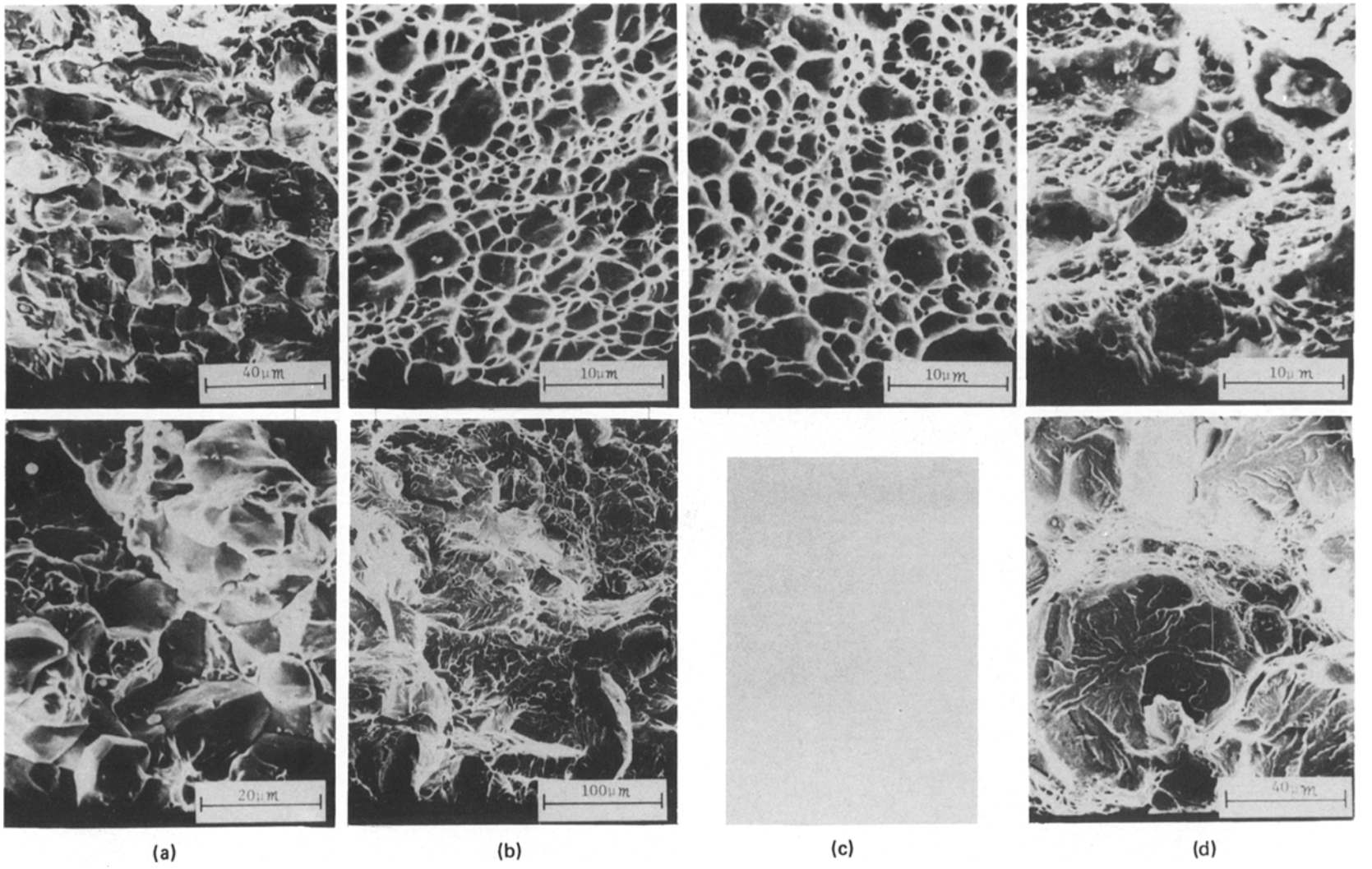

Figure 8 SEM fractographs from tensile specimens (upper) and notch bend specimens (lower) of (a) Fe–12 at % Ni, (b) Fe–12 at % Ni–0.18 at % Ti, (c) Fe–12 at % Ni–0.47 at % Ti, and (d) Fe–12 at % Ni–0.99 at % Ti alloys heat treated at 685° C and tested at – 196° C.

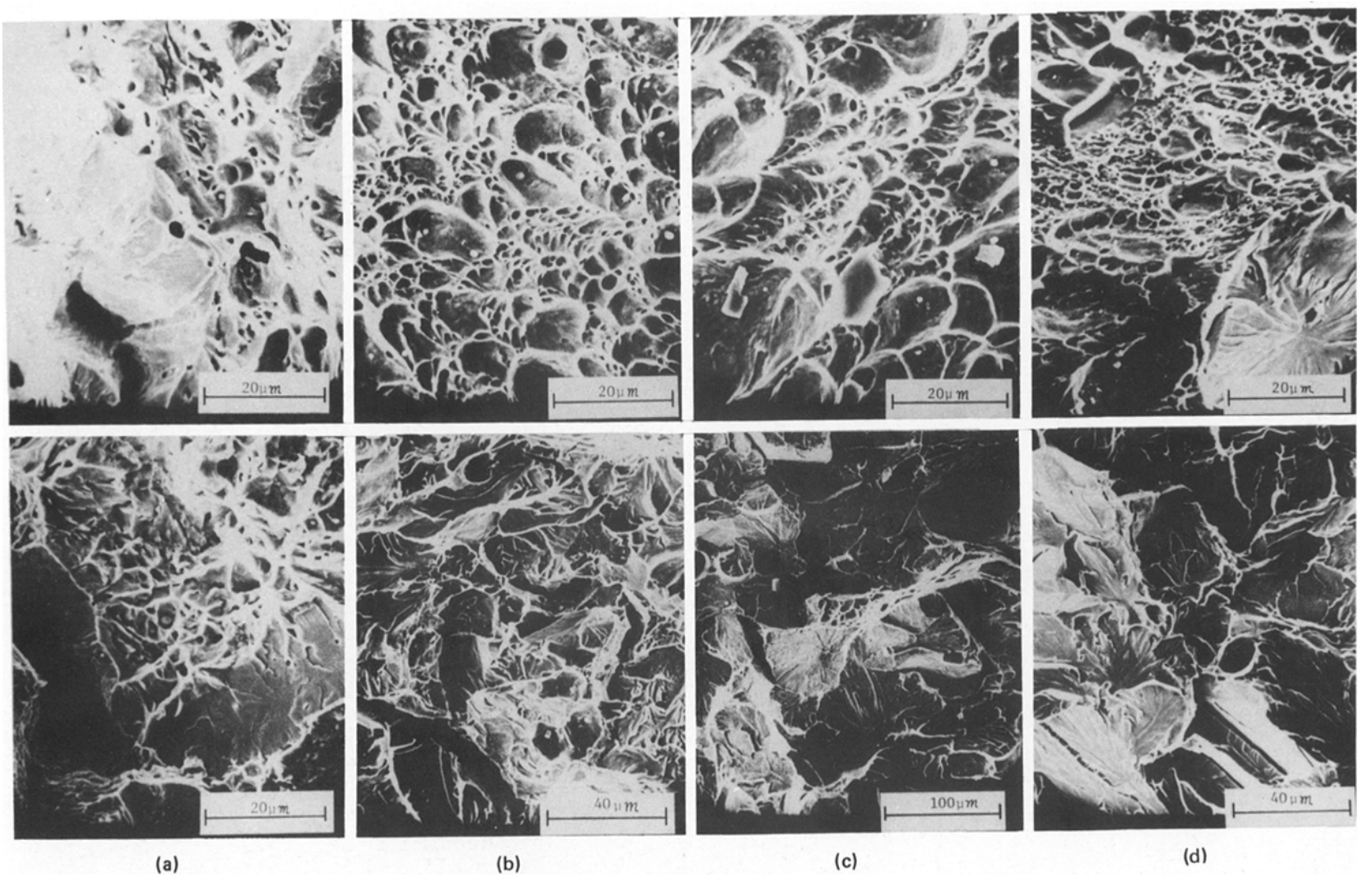

Figure 9 SEM fractographs from tensile specimens (upper) and notch bend specimens (lower) of (a) Fe–12 at % Ni, (b) Fe–12 at % Ni–0.18 at % Ti, (c) Fe–12 at % Ni–0.47 at % Ti, and (d) Fe–12 at % Ni–0.99 at % Ti alloys heat treated at 820° C and tested at — 196° C.

TABLE II Summary of SEM observations on the fracture surface of the tensile specimens tested at − 196° C

Specimen number	Nominal composition (at%)	Annealing temperature (° C)	Morphology of inclusions	Dimple size (microns)	Fracture surface characteristics
C974-T-1	Fe–12Ni	550	Spheroidal	2.54	60% cleavage fracture; 40% ductile fracture; dimple sizes are not uniform and mixed with cleavage fracture
C974-T-3	Fe–12Ni	685	Spheroidal	2.77	90% cleavage and intergranular fracture; 10% ductile fracture
C974-T-5	Fe–12Ni	820	Spheroidal and cubical	5.08	50% cleavage fracture; 50% ductile fracture; dimple sizes are not uniform
D367-T-2	Fe–12Ni–0.18Ti	550	Spheroidal and cubical	2.89	100% ductile fracture; dimple sizes are not uniform
D367-T-4	Fe–12Ni–0.18Ti	685	Spheroidal and rectangular	1.86	100% ductile fracture; dimple sizes are not uniform
D367-T-6	Fe–12Ni–0.18Ti	820	Spheroidal and cubical	2.25	100% ductile fracture; uniform uniform dimple size
D27-D-2	Fe–12Ni–0.47Ti	550	Spheroidal and rectangular	2.95	15% cleavage fracture; 85% ductile fracture
D27-T-4	Fe–12Ni–0.47Ti	685	Spheroidal and cubical	1.73	100% ductile fracture; dimple sizes are not uniform
D-27-T-6	Fe–12Ni–0.47Ti	820	Spheroidal, hexagonal and rectangular	2.37	5% cleavage fracture; 95% ductile fracture
D-141-T-2	Fe–12Ni–0.99Ti	550	Irregular shape	2.60	20% cleavage fracture; 80% ductile fracture
D-141-T-4	Fe–12Ni–0.99Ti	685	Cubical and rectangular	1.73	10% cleavage fracture; 90% ductile fracture; dimple sizes are irregular
D-141--6	Fe–12Ni–0.99Ti	820	Spheroidal	2.03	10% cleavage fracture; 90% ductile fracture

alloy heat treated at 685° C. For these particular additions and heat treatments entirely ductile fracture characterized by the occurrence of a dimpled structure, was observed. Of special significance is that all additions of Ti eliminate the intergranular fracture which occurred in the Fe–12 at% Ni base alloy. In the case of cleavage, the amount of this fracture mode is significantly reduced by the minimum Ti addition of 0.15 wt% (0.18 at%) for the 685 and 820° C heat treatments and then increases again at the higher Ti contents.

A plot of the fracture toughness against the percentage of ductile fracture for the various materials and heat treatments is given in Fig. 10. It is seen that a correlation exists between K_{IC} and the percentage of ductile fracture, suggesting that the effects of Ti additions and heat treatments are to a large extent through their effects on the fracture mode.

Inclusions ranging in size from 1 to 5 μm and with an average spacing of 20 to 50 μm were evident in all fractographs. They were for the most part spheroidal in shape in the Fe–12 at% Ni base alloy and cubic or rectangular in the alloys with Ti additions, the relative number of the latter two shapes increasing with increase in Ti content.

Upon comparing the fractographs of broken tensile specimens with those of the fracture toughness specimens, it was found that the tensile specimens exhibited a higher percentage of ductile fracture and a smaller dimple size than the fracture toughness specimen. Also, the dimple size in the tensile specimens was independent of heat treatment temperature while that in the fracture toughness specimens increased with heat treatment temperature. The size, shape and averaging spacing of the inclusions in the two types of specimens were similar.

3.3. Transmission electron microscopy (TEM)

Typical TEM micrographs of the Fe–12 at% Ni

TABLE III Summary of SEM observations on the fracture surface of the fracture toughness specimens tested at −196° C

Specimen number	Nominal composition (at%)	Annealing temperature (° C)	Morphology of inclusions	Dimple size (microns)	Fracture surface characteristics
C974-B-1	Fe–12Ni	550	Spheroidal	3.54	80% cleavage fracture; 20% ductile fracture
C974-B-3	Fe–12Ni	685	Spheroidal	not measurable	98% cleavage and intergranular fracture; 2% ductile fracture
C974-B-5	Fe–12Ni	820	Spheroidal	not measurable	90% cleavage and intergranular fracture; 10% ductile fracture
C367-B-2	Fe–12Ni–0.18Ti	550	Spheroidal and cubical	1.71	90% cleavage fracture; 10% ductile fracture
C367-B-4	Fe–12Ni–0.18Ti	685	Spheroidal	6.49	50% cleavage fracture; 50% ductile fracture
C367-B-6	Fe–12Ni–0.18Ti	820	Spheroidal and cubical	7.68	50% cleavage fracture; 50% ductile fracture
D27-B-2	Fe–12Ni–0.47Ti	550	Rectangular	not measurable	98% cleavage fracture; 2% ductile fracture
D27-B-6	Fe–12Ni–0.47Ti	820	Cubical and rectangular shape	8.82	50% cleavage fracture; 50% ductile fracture
D141-B-2	Fe–12Ni–0.99Ti	550	Irregular shape	not measurable	100% cleavage fracture
D141-B-4	Fe–12Ni–0.99Ti	685	Spheroidal and rectangular	3.45	80% cleavage fracture; 20% ductile fracture
D141-B-6	Fe–12Ni–0.99Ti	820	Small spheroidal	11.06	80% cleavage fracture; 20% ductile fracture

base alloy and of the Fe–12 at% Ni–0.18 at% Ti alloy heat treated at the three designated temperatures are presented in Fig. 11. In all cases a cellular type of dislocation structure was produced in which there exists regions with a high density of dislocations mixed with areas almost devoid of dislocations. The total density of dislocations tended to increase with increase in heat treatment temperature. A fine precipitate occurs in the Fe–12 at% Ni–0.18 at% Ti alloy heat treated at 550° C, whereas there is no evidence of a precipitate in this alloy heat treated at 685 and 820° C.

3.4. Auger electron spectroscopy

Auger spectrum mappings for the elements Fe, Ni, Ti, C, N and O on the fracture surfaces of the broken fracture toughness specimens tested at −196° C were obtained. Each mapping gives the characteristic intensity distribution for the designated element and provides an indication of the relative affinity between the various elements in a particular alloy. The affinities deduced from the mappings are summarized in Table IV. The results indicate the following: (a) Nickel is always associated with the iron. (b) For the Fe–12 at% Ni base alloy heat treated at 550° C, the interstitials N and O are rather uniformily distributed, whereas C tends to avoid regions with high concentrations of Fe and Ni. When the heat treatment temperature is increased to 685° C, C tends to associate with O but still avoids Fe and Ni. (c) For the Fe–12 at% Ni–x at% Ti alloys heat treated at 550 and 685° C, the interstitials C, N and O tend to occur in regions where the Ti atoms are located, the tendency increasing with increase in heat treatment temperature. Upon increasing the heat treatment temperature to 820° C, a stronger association of N with Ti occurs, but O and C occur in regions of low Ti content. (d) The association of Ni with Ti only occurs for the Fe–12 at% Ni–0.18 at% Ti alloy heat treated at 550° C and the Fe–12 at% Ni–0.99 at% Ti alloy heat treated at 820° C.

4. Discussion

As pointed out above, Witzke and Stephens [5] found that maximum K_{IC} occurred for the Fe–12 at% Ni–0.18 at% Ti alloy heat treated at 685° C. Since the present studies have shown that

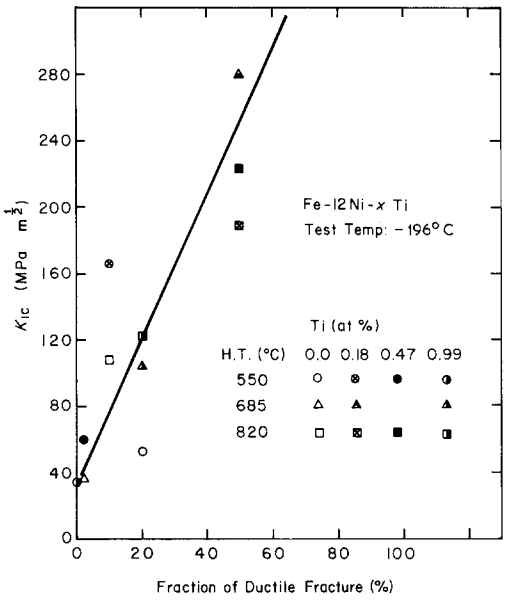

Figure 10 K_{IC} against the fraction of ductile fracture at − 196° C for Fe–12 at% Ni–x at% Ti alloys heat treated at 550, 685 and 820° C.

K_{IC} for the various titanium additions and heat treatments correlates with the percentage of ductile fracture, the effects of the Ti additions and heat treatments may be explained in terms of their influence on the fracture mode. The fact that maximum fracture toughness already occurred for the smallest Ti addition (0.18 at%) is then explained as follows. A simple calculation shows that this amount of Ti is sufficient to combine with all of the interstitial atoms which are present to form simple Ti compounds. The cubic and rectangular inclusions observed in the SEM fractographs are probably these compounds formed during the gettering of the melt. Upon forming these compounds, the concentration of deleterious interstitials (probably oxygen) at the grain boundaries is reduced to the point where their weakening effect is eliminated and intergranular fracture no longer occurs. The decrease in toughness with further additions of Ti beyond 0.18 at% is then probably due to the fact that such additions produce an increase in the flow stress and at the same time cause a slight decrease in the fracture stress, thereby leading to an earlier (strain-wise) intersection of the flow stress curve with the fracture stress curve. This then often leads to an decrease in the true fracture strain ϵ_F and the work of fracture W_F, and in turn the fracture toughness, since K_{IC} was found to correlate with ϵ_F and W_F. The increase in flow stress with the addition of Ti could be due to an increase in the amount of the precipitate (probably Ni_3Ti or Fe_2Ti) which was observed for the 550° C heat treatment and to a reduction in the fineness of the microstructure associated with the $\gamma \rightarrow \alpha$ transformation. The influence of the heat treatment temperature might then also be through its effect on the amount, size and distribution of the precipitate and on the dislocation structure and other microstructural features produced by the $\gamma \rightarrow \alpha$ transformation. Additional detailed TEM studies are needed to more fully evaluate the microstructural changes and their possible influence on K_{IC}.

The Auger electron spectroscopy mappings of the fracture surfaces indicated that the interstitials C, N and O were only weakly associated with the Ti atoms for the 550 and 685° C heat treatments. Upon increasing the heat treatment temperature to 820° C the association between the N and Ti atoms became stronger, whereas that for the other two interstitials became weaker. This preference of Ti for N is in accord with estimates [11] of the bond energies between Ti and the interstitials C, N and O; see Table V. It is seen from this table that for each type of measurement the bonding energy between the Ti and N atoms is slightly higher than that for the other two interstitials.

The Auger mappings did not provide any clear evidence for the existence of the inclusions which were observed in the SEM fractographs, nor of the precipitates observed by TEM. This was probably due to the small size of these particles, which was between 1 and 5 μm in the case of the inclusions and less than 1 μm in the case of the precipitates. These sizes are near or below the resolving power of the Auger mapping system and hence would not normally show up.

Of additional interest is the fact that only rarely was an inclusion seen in the TEM observations, whereas such inclusions were abundantly evident in the SEM fractographs. A simple calculation based on the average spacing of the inclusions in the SEM fractographs indicated that the probability of seeing one at the magnification employed in TEM was about one in a thousand.

5. Summary

Witzke and Stephens [5] studied the effects of minor additions of Ti (0.18 to 0.99 at%) on the fracture toughness at − 196° C of a Fe–12 at% Ni

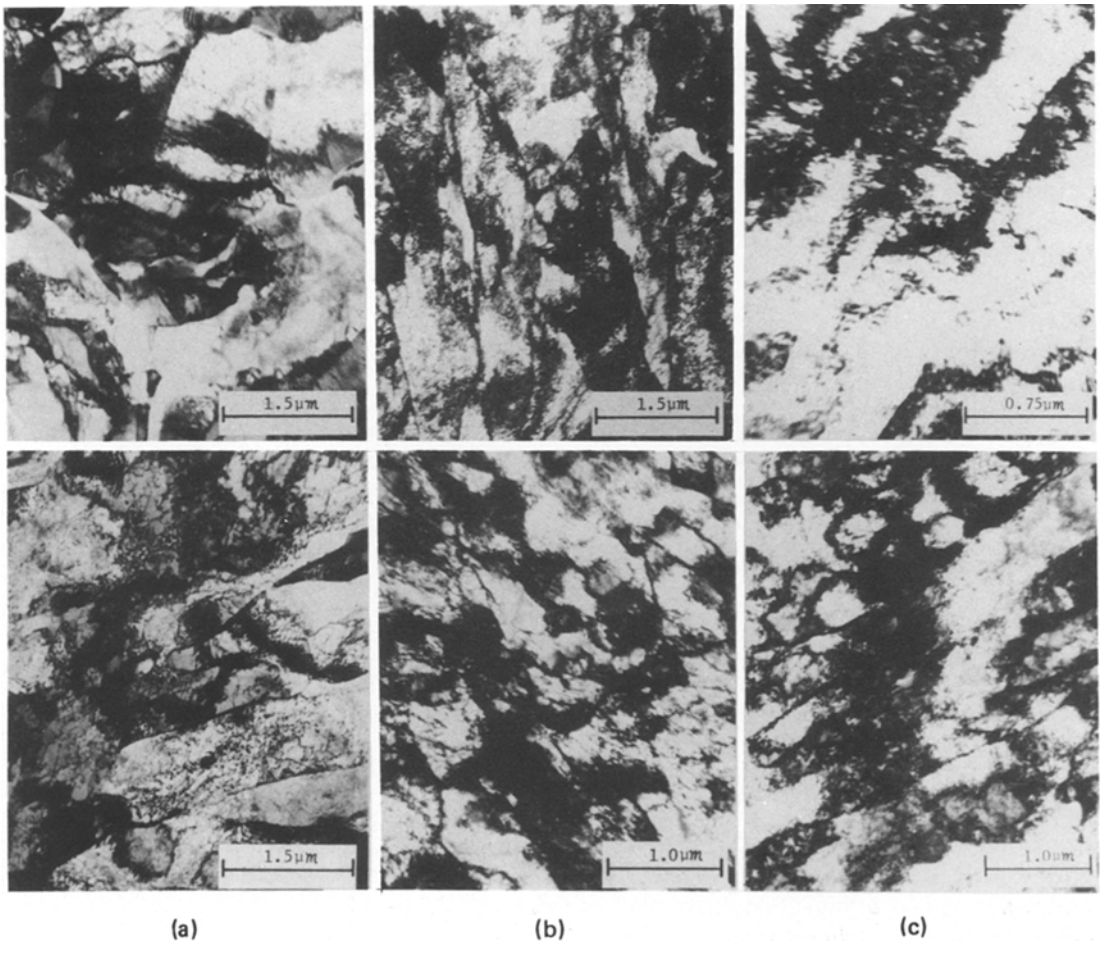

Figure 11 TEM micrographs from Fe–12 at % Ni (upper) and Fe–12 at % Ni–0.18 at % Ti (lower) specimens heat treated at (a) 550° C, (b) 685° C and (c) 820° C.

TABLE IV Relative affinities of the elements in Ti–12 at % Al–x at % Ti alloys determined from Auger mappings

Nominal composition (at %)	Degree of association			Moderate dissocation	Relatively uniform distribution	Non-uniform distribution Assoc. or Dissoc.
	Strong	Moderate	Weak			
550° C 2 h, water quenched						
Fe–12Ni	Ni, Fe	–	–	C (Fe, Ni)	O, N	–
Fe–12Ni–0.18Ti	Ni, Fe	–	Ni, Ti, C, O	–	N	–
Fe–12Ni–0.47Ti	Ni, Fe	–	Ti, C, O	–	O	–
685° C 2 h, water quenched						
Fe–12Ni	Ni, Fe	–	–	C (Fe, Ni)	N	C, O
Fe–12Ni–0.18Ti	Ni, Fe	–	–	Ti, C, N, O	–	–
Fe–12Ni–0.99Ti	Ni, Fe	–	–	T, C, N, O	–	–
820° C 2 h, water quenched						
Fe–12Ni–0.18Ti	Ni, Fe	Ti, N	–	–	–	O, C
Fe–12Ni–0.47Ti	Ni, Fe	Ti, N	–	C (Fe, Ni)	–	O
Fe–12Ni–0.99Ti	Ni, Fe	Ti, N	O, C	–	–	–

TABLE V Summary of bond energies, e, for TiO, TiN and TiC compounds determined by various methods and the activation energy for diffusion, Q_D, for dilute solutions of the interstitial solutes in Ti. All energies in eV. (From Conrad [11])

System	Bond energy, e derived from			Activation energy for diffusion, Q_D (eV)
	ΔH^θ	ΔH_s	γ_s	
Ti–O	2.13	1.17	1.17	2.18
Ti–N	2.22	1.70	1.42	2.50
Ti–C	2.18	1.25	1.13	2.00

Notes: ΔH^θ = Heat of formation, ΔH_s = Heat of sublimation and γ_s = Surface energy.

base alloy heat treated at 550, 685 and 820° C respectively and found that maximum K_{IC} occurred for addition of 0.18 at% Ti heat treated at 685° C. The following is a summary of the more significant findings of the present investigation, using TEM, SEM and Auger electron spectroscopy, into the reasons for this improvement in K_{IC}.

1. K_{IC} at −196° C for all alloys and heat treatments considered here correlated with the fraction of ductile fracture compared to intergranular and cleavage fracture, the latter modes being predominant in the Fe–12 at% Ni base alloy without Ti additions.

2. Inclusions 1 to 5 μm in size and 20 to 50 μm spacing were noted in the SEM fractographs of both tensile and fracture toughness specimens tested at −196° C. The inclusions were spheroidal in shape in the Fe–12 at% Ni base alloy, but were for the most part cubic or rectangular in the Fe–12 at% Ni–x at% Ti alloys.

3. A fine precipitate was observed by TEM in the Fe–12 at% Ni–0.18 at% Ti alloy heat treated at 550° C; this precipitate was not seen for the 685 and 820° C heat treatments of this particular alloy.

4. Auger mappings indicated a weak to moderate association of the interstitials C, N and O with Ti, the degree of which depended on the particular interstitial element and the heat treatment temperature.

5. The following explanations were inferred from the results obtained: (a) The increase in K_{IC} resulting from the initial addition of 0.18 at% Ti is due to: (i) the scavenging of interstitials which normally segregate to the grain boundaries and (ii) refining of the microstructure, making cleavage more difficult. (b) The subsequent decrease in K_{IC} for Ti addition > 0.18 at% is due to the increase in flow stress resulting from these additions and a slight decrease in fracture stress, which in turn leads to an earlier intersection of the flow curve with the cleavage fracture stress curve. (c) The effects of the Ti additions and heat treatment temperature on K_{IC} is partly due to their influence on the amount, size and distribution of the precipitate which was observed at 550° C.

References

1. J. A. RINEBOLT and W. J. HARRIS, Jr, *Trans. Amer. Soc. Met.* **43** (1951) 1175.
2. E. A. STEIGERWALD and C. VISHNEVSKY, Literature Survey on the Influence of Alloy Elements on the Fracture Toughness of High Strength Steels, Thompson Ramo Woolridge Co., Inc (AMMRC-CR-67-13(F) AD-665432) (1968).
3. W. P. REES and B. E. HOPKINS, *J. Iron and Steel Inst.* **172** (1952) 403.
4. F. P. PICKERING, "The Effect of Composition and Microstructure on Ductility and Toughness. Symposium: Toward Improved Ductility and Toughness", (Climax Molybdenum Development Co. (Japan) Ltd., Tokyo, 1970) p. 9.
5. W. R. WITZKE and J. R. STEPHENS, "Effect of Minor Reactive Metal Additions on Fracture Toughness of Iron-12 Per cent Nickel Alloy at −196° C and 25° C", National Aeronautical and Space Agency TN D-8232, May 1976.
6. S. JIN, J. W. MORRIS, Jr and V. F. ZACKAY, *Advan. Cryog. Eng.* **19** (1974) 379.
7. F. W. JONES and W. I. PUMPHREY, *J. Iron Steel Inst.* **163** (1949) 121.
8. G. SASAKI, D. Eng. Thesis, University of California, Berkeley, California, 1973.
9. S. JIN, J. W. MORRIS, Jr and V. F. ZACKAY, *Met. Trans.* **6A** (1975) 141.
10. P. W. PALMBERG, *J. Vacuum Sci. Technol.* **9** (1972) 160.
11. H. CONRAD, *Prog. Mater. Sci.* (1981).

Received 14 April and accepted 30 June 1980.